20th Australasian Fluid Mechanics Conference
Perth, Australia
5-8 December 2016

Aerodynamic Hovering Performance of Rigid and Flexible Wing Planform Shapes

A. Shahzad, F.B. Tian, J. Young, and J.C.S. Lai

School of Engineering and Information Technology
The University of New South Wales, Canberra, ACT 2600, Australia

Abstract

Wing geometric parameters govern the aerodynamic performance of insects and micro aerial vehicles. Previous studies of wing shapes have been limited to rigid wings. The aerodynamic hovering performance of rigid and flexible wing shapes for aspect ratio AR = 1.5 is evaluated computationally at the Reynolds number (Re) of 400. The three-dimensional viscous incompressible Navier-Stokes equations are solved for rigid wing simulations using a sharp interface immersed boundary method (IBM) coupled with an in-house non-linear finite element based structure solver for flexible wing simulations. The wing shapes with different area distributions along the span are defined by the radius of the first moment of wing area ($\bar{r}_1$). We model $\bar{r}_1$= 0.43, 0.53 and 0.63 wings using a beta distribution. The results show that for a given shape, the flexible wing produces higher mean lift coefficient ($\overline{C_L}$) at the cost of the power economy (PE, defined as the ratio between mean lift and aerodynamic power coefficients). Compared to the rigid wing, deformation in a high $\bar{r}_1$ flexible wing results in large variation in the pitch angle during flapping. Consequently, $\overline{C_L}$ is high during supination and pronation accompanied by a drop in $\overline{C_L}$ during the stroke reversal. Flexible wings produce a wider range of lift but require higher peak aerodynamic and inertial power inputs. For a given $\overline{C_L}$, flexible wings require smaller $\bar{r}_1$ to produce the same aerodynamic performance as rigid wings.

Introduction

Inspired by extraordinary flapping flight modes found in nature, researchers continue to explore insect flight for developing insect-like micro aerial vehicles (MAV). The parameters of wing geometry, flexibility and kinematics are the key drivers of lift enhancement and flight efficiency. In this work, the scope is limited to the role of wing geometry (planform shapes only) and flexibility in hover.

Phillips et al. [10] noticed similar flow topology on rigid generic wing shapes such as an ellipse, four ellipse, reverse ellipse and rectangle. Likewise, Ozen and Rockwell [9] also reported similar flow structures on the rectangular and fruit fly wings in their experiments. Consistent with these findings, the computational work of Luo and Sun [6] found less than 5% difference in the force coefficients of ten wing shapes based on a fruit fly wing. However, Ansari et al. [1] and Wilkins [13] mentioned that the wings with more area outboard, that is, towards the wing tip, produce more lift at the cost of high power requirements. In our previous computational work [11], the performance of $\bar{r}_1$= 0.43, 0.53, 0.63 and rectangular wing was compared at Re = 12, 400 and 13500. We found that despite the changes in flow structures like leading edge vortex (LEV), trailing edge vortex (TEV), root vortex (RV) and tip vortex (TV) at different Re, the performance trends remain Re independent. The $\bar{r}_1$= 0.43 wing is found to be the most efficient in terms of PE.

It is worth mentioning that all the studies of wing planform shapes have been conducted with an assumption of the wings being rigid and a detailed analysis of flexible wing shapes has yet to be carried out. The aim of this study is to investigate the aerodynamic performance of rigid and flexible wing shapes at Re = 400, based on the mean chord length (c) and wing tip velocity (U_{tip}), to represent a range of insects and MAV. This work will not only improve our understanding of insect flight but also help in designing better wings for MAV.

Wing Geometry and Kinematics

The beta distribution wings [5] defined by $\bar{r}_1$ are a reasonable approximation of the wings of insects. We model $\bar{r}_1$ = 0.43, 0.53 and 0.63 wings presented in figure 1, to represent a variety of wing shapes found in nature. For the simulation of rigid wings, the flexible part is also taken as rigid. A larger $\bar{r}_1$ indicates greater wing area towards the wingtip.

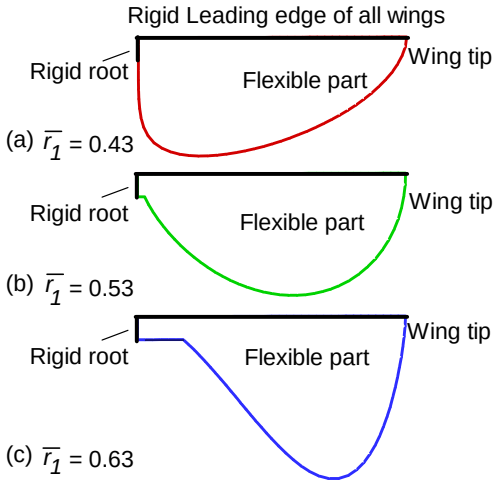

Figure 1. Wing shapes.

Unlike real insects, the $\bar{r}_1$ = 0.63 beta distribution wing has a pointed wing root as shown in figure 2. In order to make it closer to nature, the root shape has been modified, resulting in a small increase of approximately 3% in the area and AR. Since the wing root is close to the pivot point, this modification is not expected to influence the aerodynamic performance of the wing significantly.

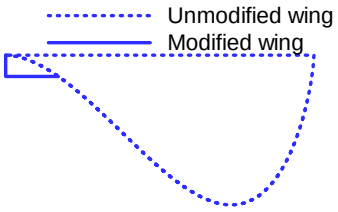

Figure 2. Modification of wing root on $\bar{r}_1$ = 0.63 wing.

For simplification, we have assumed rigid leading edge (LE) and wing root (up to 0.25c from the LE) for fluid-structure interaction

(FSI) simulations, noting that the root and LE are the stiffest parts of insect wings [3, 4]. Future work will incorporate more realistic models of spanwise variation of leading-edge stiffness. The mass ratio (m^*) in equation (1), and the effective stiffness (π_1) in equation (2) are taken as 4 and 14 respectively. While this value of m^* is representative of a Hawkmoth, π_1 has been chosen such that the wing deformation is not influenced by structural resonance. The Poisson's ratio (ν) of 0.3, defined as the ratio between the transverse and axial strain, is used for the computations [3].

$$m^* = \rho_s h_s / \rho_f c \quad (1)$$

$$\pi_1 = E {h_s}^3 / [12c^3(1-\nu^2)\rho_f {U_{tip}}^2] \quad (2)$$

where ρ_f and ρ_s are the fluid and structure densities, h_s the wing thickness and E the Young's modulus.

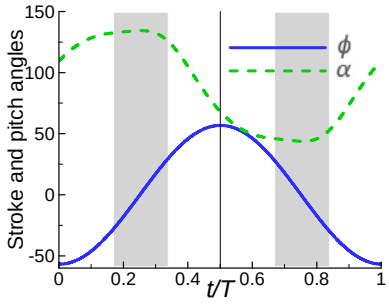

Figure 3. Wing kinematics [10]. Grey shaded portion of t/T = 0.17-0.34 and t/T = 0.67-0.84 shows the mid up and mid down strokes respectively.

The advanced flip kinematics of Phillips [10] shown in figure 3 have been used in the study. The advanced flip refers to the change in the orientation of the pitch angle before the stroke reversal at t/T = 0.5. The wing flaps in a horizontal stroke plane with a stroke angle (ϕ) defined by the sinusoidal function and it rotates about the LE with a pitch angle (α) defined by the Fourier series. The stroke amplitude and the flapping frequency are 56.35º and 20 Hz respectively.

Computational Method

The numerical method is based on a sharp interface IBM [12] in which the viscous and incompressible Navier-Stokes equations are discretized on a non-uniform Cartesian grid shown in figure 4. The flow is assumed to be laminar and the fluid domain is a cube of 25c. For FSI simulations, the fluid dynamics is combined with the structure dynamics through the boundary conditions of no-slip, no penetration and traction conditions. The spars and membranes are approximated with frames and plates respectively. The stability of FSI coupling is improved by using implicit coupling based on staggered sub-iterations. Further details of the FSI solver can be found in Tian et al. [12].

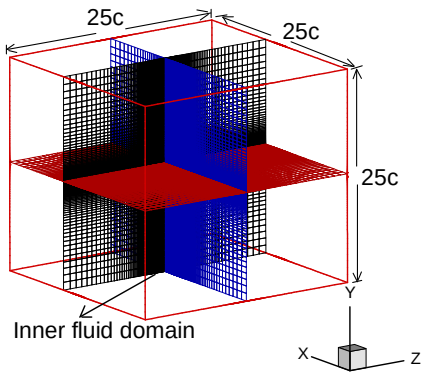

Figure 4. Computational domain.

Validation

Grid independence and time independence studies are conducted using a rigid $\bar{r_1}$ = 0.63 wing. The outer fluid domain has 50 points in x, y and z directions. For grid independence, the mesh density of the inner fluid domain is varied and for time step independence, the medium mesh is run with 1000, 2000 and 3000 time steps per flapping cycle.

Grid	No of time steps per cycle	No of cells in inner domain mesh	$\overline{C_L}$	$\overline{C_{Pa}}$
1. Grid independence				
Coarse	2000	32 × 30 × 54	1.064	2.423
Medium		44 × 42 × 78	1.082	2.550
Fine		62 × 60 × 108	1.085	2.630
2. Time independence				
Medium	1000	44 × 42 × 78	1.102	2.633
	2000		1.079	2.548
	3000		1.068	2.508

Table 1. Results of grid independence and time step independence studies

The results in table 1 indicate that the difference is within 3% for the average lift coefficient ($\overline{C_L}$) and average aerodynamic power coefficient ($\overline{C_{Pa}}$), between the medium and the fine grid. The medium grid with 2000 and 3000 time steps/cycle also gives less than 3% variation in the results. Therefore, the medium grid with 2000 time steps/cycle was chosen for the simulations.

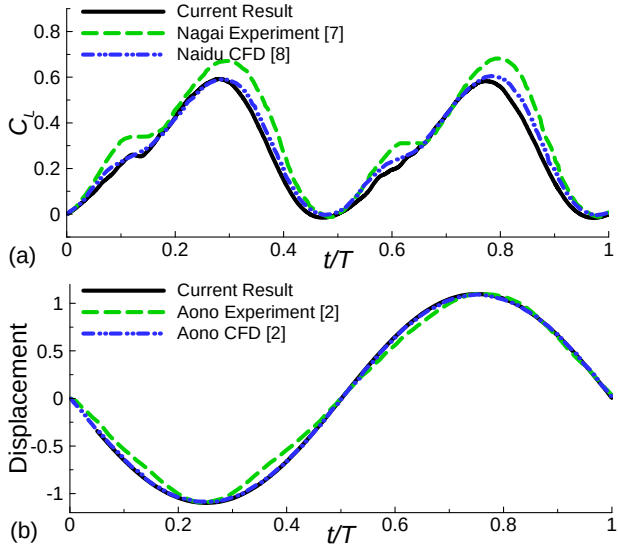

Figure 5. (a) Fluid solver validation and (b) FSI solver validation.

The fluid solver validation is performed against the experiments of Nagai et al. [7] and the computational study of Naidu et al. [8]. The time histories of the lift coefficient (C_L) in figure 5(a) indicate that our simulations are in good agreement with both the experimental and CFD results. In the FSI solver validation, the time history of wing tip displacement normalized by the root chord given in figure 5(b) also matches well with both the experimental and CFD results of Aono et al. [2].

Results and Discussions

In this section, the detailed analysis of the performance of wing shapes is presented. The time histories of C_L in figure 6(a) show an increase in the peak lift with $\bar{r_1}$ for both the rigid and the flexible wing shapes. The flexible wings produce higher peak lift than their rigid equivalents and this increase is approximately 22%, 26% and 28% for the $\bar{r_1}$ = 0.43, 0.53 and 0.63 wings respectively. Moreover, there is a significant change in the timing

of peaks for the flexible $\bar{r}_1$ = 0.63 wing. For instance, in the up stroke, while the first and second lift peaks in the rigid $\bar{r}_1$ = 0.63 wing occur at t/T = 0.143 and 0.335 respectively, the first peak in the corresponding flexible wing occurs early, by t/T = 0.05, and the second one with a delay, by t/T = 0.05. All the wings attain zero lift before the stroke reversal, between t/T = 0.436 and 0.455, because of advanced flip kinematics. The minimum lift for the rigid and flexible $\bar{r}_1$ = 0.63 wings has a time difference of about t/T = 0.023, as the flexible wing achieves a minimum lift of -1.879 at t/T = 0.491, very close to the stroke reversal. This minimum lift is 82.2% less in magnitude than the corresponding rigid wing.

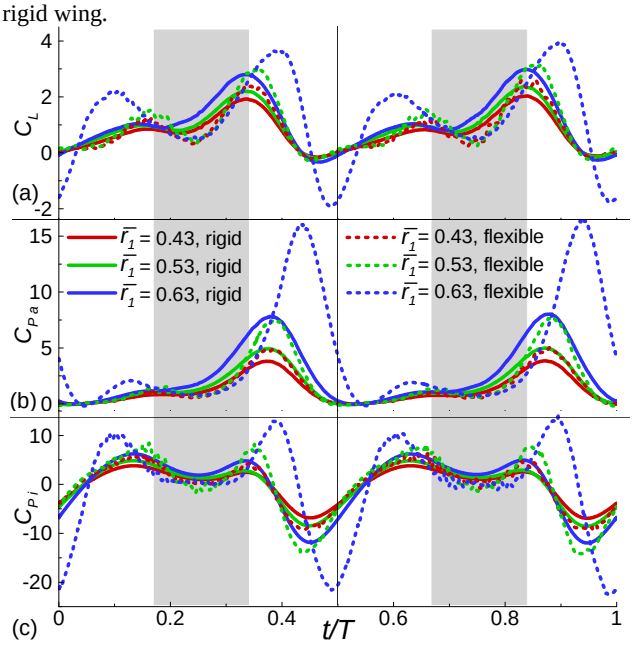

Figure 6. Time history of (a) C_L , (b) C_{Pa} and (c) C_{Pi} of all wings.

Similar to the peak C_L, the peak aerodynamic power (C_{Pa}) and the peak inertial power (C_{Pi}) also increase with an introduction of flexibility for all wing shapes. This increase in C_{Pa} is 21%, 33%, 52% and C_{Pi} is 41%, 61%, 63% for the $\bar{r}_1$ = 0.43, 0.53 and 0.63 wings, respectively. Compared with low $\bar{r}_1$ wings, there is a drastic increase in power requirements for the flexible $\bar{r}_1$ = 0.63 wing. Since there is a phase difference between the inertial and aerodynamic forces during a flapping cycle, the inertial and aerodynamic power requirements vary over a flapping cycle. Since the $m^*$of flexible wings is high, the wing deformation is mainly governed by the inertial effects. With less fluid damping, it is not surprising to observe higher inertial power requirement for flexible wings.

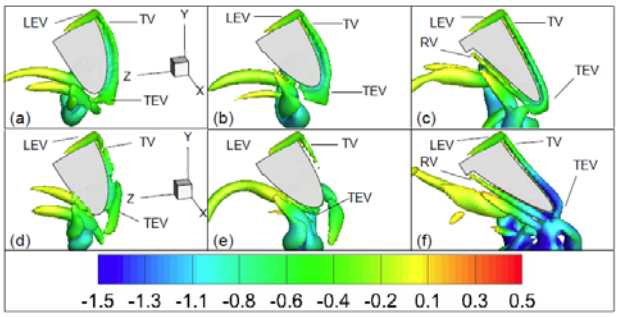

Figure 7. Iso-Q surfaces filled with pressure coefficients at t/T = 0.1 on (left) $\bar{r}_1$ = 0.43, (centre) $\bar{r}_1$ = 0.53 and (right) $\bar{r}_1$ = 0.43 wings. (a-c) rigid wings and (d-f) flexible wings.

The flow features on the wings are visualized at t/T = 0.1, 0.4 and 0.5 using the iso Q-surfaces (Q = 10) filled with the pressure coefficients. Here the strength of the vortices is defined qualitatively in terms of the suction pressure coefficients. As the leading edge of the flexible wings is assumed rigid, the LEV of rigid and flexible wings for a given shape is similar and the difference in lift and power with flexibility is attributable to the TEV, RV, and TV structures.

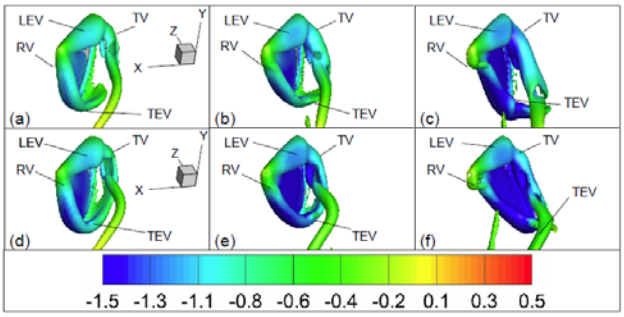

Figure 8. Iso-Q surfaces filled with pressure coefficients at t/T = 0.4 on (left) $\bar{r}_1$ = 0.43, (centre) $\bar{r}_1$ = 0.53 and (right) $\bar{r}_1$ = 0.43 wings. (a-c) rigid wings and (d-f) flexible wings.

In figure 7, at t/T = 0.1, the wings are at the start of the up stroke. Here the rigid $\bar{r}_1$ = 0.43 and 0.53 wings produce more lift because their TEV and TV (figure 7(a and b)) have developed earlier than the flexible wings (figure 7(d and e)). In contrast, the rigid $\bar{r}_1$ = 0.63 wing produces comparatively less lift than the flexible wing because the large deformation of trailing edge in the flexible wing results in a very strong TV and TEV (figure 7(f)). These observations are consistent with the trend of C_L in figure 6(a).

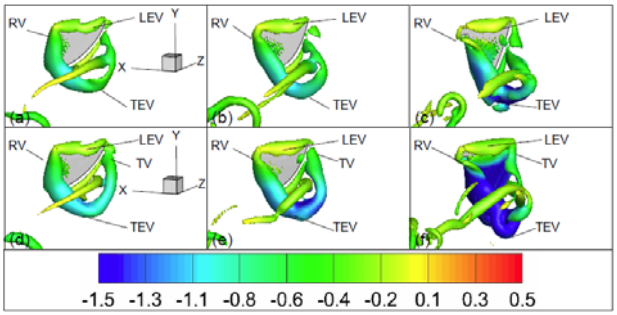

Figure 9. Iso-Q surfaces filled with pressure coefficients at t/T = 0.5 on (left) $\bar{r}_1$ = 0.43, (centre) $\bar{r}_1$ = 0.53 and (right) $\bar{r}_1$ = 0.43 wings. (a-c) rigid wings and (d-f) flexible wings.

In figure 8, at t/T = 0.4, the wing is about to reach the end of the up stroke as it also pitches about the LE to change direction during pronation. At this moment, all the flexible wings produce greater C_L in figure 6(a) than the corresponding rigid wings. The iso-Q surfaces show that the TV of all the wings, except the flexible $\bar{r}_1$ = 0.63 (figure 8(f)), is detached or about to detach from the wing tip at this time instant. Flexibility results in an induced negative camber in the flexible $\bar{r}_1$ = 0.63 wing which helps in keeping the strong TEV and TV close to the wing surface. This results in a comparatively high C_L of flexible $\bar{r}_1$ = 0.63 wing. At t/T = 0.5, as the wing approaches a stroke reversal, the pitch angle is 68.3º and the LEV, TEV, TV, and RV are all on the underside of the wings. Therefore, there is almost zero or negative lift (figure 6(a)) on all the wings. While the TV and TEV are detached from the rest of the wings, there is a strong region of very low pressure, seen in figure 9(f), on the underside of the flexible $\bar{r}_1$ = 0.63 wing that results in a C_L of -1.72. It is the same TEV structure that produced a high C_L on this wing at t/T = 0.4 in figure 8(f).

It is evident from the above analysis that the wing shape and flexibility influences the production of forces and the requirement of aerodynamic and inertial power during a flapping cycle. The effects of flexibility are more pronounced on high $\bar{r}_1$

wings because there is more area close to the wing tip, where the flapping velocity and the bending moments are high. Higher lift associated with high $\bar{r}_1$ rigid and flexible wings is accompanied by high power requirements. While comparing the time histories of lift of the rigid and flexible wings equivalents in figure 6(a), clearly, there are different phases in the flapping cycle, where one dominates over the other. For example, in a half stroke (t/T = 0-0.5), comparatively more lift in a flexible $\bar{r}_1$ = 0.63 wing at t/T = 0.035-0.185 and t/T = 0.345-0.455 is significantly offset by relatively less lift at t/T = 0-0.035 and t/T = 0.185-0.345. Therefore, it is useful to consider the mean values for these cases. In addition, the power economy (PE) defined in equation (3) is used to measure the efficiency of lift production of the hovering wings.

$$PE = \overline{C_L} / \overline{C_P} \quad (3)$$

The $\overline{C_L}$ in figure 10(a) shows an increase with $\bar{r}_1$ for both the rigid and flexible wings. In comparison with rigid, the high $\bar{r}_1$ flexible wing ($\bar{r}_1$ = 0.63) exhibits a greater increase in $\overline{C_L}$, however, it is clearly at the cost of high PE. For hover, the wing should ideally use minimum input power and produce enough lift to support the weight of the insect at the same time. The PE plotted against the $\overline{C_L}$ as a function of $\bar{r}_1$ in figure 10(b) helps us to determine efficient wing shapes. It is observed that the flexible wing shapes cover a wider range of lift and give PE comparable to the rigid wing shapes. For a given $\overline{C_L}$, a flexible wing with comparatively lower $\bar{r}_1$ than the rigid wing can give similar PE. For instance, a rigid wing with $\bar{r}_1$ of about 0.57 and a flexible wing with $\bar{r}_1$ of 0.53 can both give a $\overline{C_L}$ of 0.96 while maintaining PE of 0.5. It is, thus, preferable to use low $\bar{r}_1$ wings, if flexibility is taken into account.

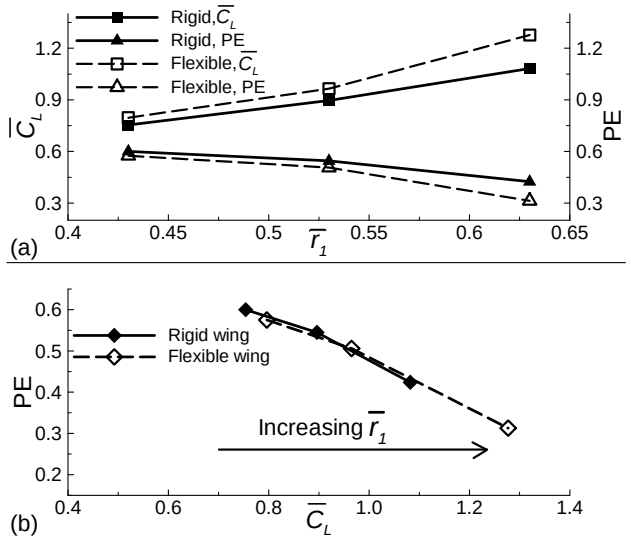

Figure 10. (a) $\overline{C_L}$ and PE vs. $\bar{r}_1$ and (b) PE vs. $\overline{C_L}$ for different wings.

Conclusion

Based on insect-inspired kinematics, we studied the effect of wing shapes and flexibility on the hovering performance of wings using a sharp interface IBM coupled with a structure dynamics solver for FSI simulations. Our results show that for a given wing, flexibility improves the lift production, but requires more aerodynamic and inertial power inputs. For both the rigid and flexible wings, high $\bar{r}_1$ gives higher peak lift and $\overline{C_L}$ at the cost of high peak input aerodynamic and inertial powers. For flexible wings, especially the $\bar{r}_1$ = 0.63, the timings and magnitude of lift vary as the high lift peak during the up stroke and down stroke are accompanied by negative lift at the commencement of each stroke. The wing deformation in flexible wings strongly affects the lift force production and power requirements as it changes the time evolution of TV and TEV structures during a flapping cycle. It is further concluded that the flexible wings require lower $\bar{r}_1$ than their rigid equivalents to maintain the required lift with almost no loss in PE.

Acknowledgment

This work was supported under the Australian Research Council's Discovery Projects funding scheme (project number DP130103850), and conducted with the assistance of resources from the National Computational Infrastructure (NCI), which is supported by the Australian Government. Aamer Shahzad acknowledges the support of NUST, Islamabad, Pakistan, via the Prime Minister's Gold Medal Scholarship and SEIT, UNSW, Canberra, which provided a top-up scholarship.

References

[1] Ansari, S.A., Knowles, K. & Zbikowski, R., Insectlike flapping wings in the hover part II: Effect of wing geometry, *Journal of Aircraft*, **45**(6), 2008, 1976-1990.

[2] Aono, H., et al., A computational and experimental study of flexible flapping wing aerodynamics, *48th AIAA aerospace sciences meeting including the new horizons forum and aerospace exposition*, 2010.

[3] Combes, S. & Daniel, T., Flexural stiffness in insect wings II. Spatial distribution and dynamic wing bending, *Journal of Experimental Biology*, **206**(17), 2003, 2989-2997.

[4] Combes, S.A. & Daniel, T.L., Flexural stiffness in insect wings I. Scaling and the influence of wing venation, *Journal of Experimental Biology*, **206**(17), 2003, 2979-2987.

[5] Ellington, C., The aerodynamics of insect flight. II. Morphological parameters, *Phil. Trans. R. Soc. Lond. B*, **305**, 1984, 17-40.

[6] Luo, G. & Sun, M., The effects of corrugation and wing planform on the aerodynamic force production of sweeping model insect wings, *Acta Mechanica Sinica*, **21**(6), 2005, 531-541.

[7] Nagai, H., Isogai, K. & Fujimoto, T., Experimental study on flow interaction between fore and hindwings of dragonfly in hovering and forward flight, *27th Congress of International Council of the Aeronautical Sciences*, 2010. Nice, France.

[8] Naidu, V., Young, J. & Lai, J., Effect of wing flexibility on the performance of tandem wings during hover flight, *31st AIAA Applied Aerodynamics Conference*, 2013. San Diego, CA.

[9] Ozen, C. & Rockwell, D., Flow Structure on a Rotating Wing: Effect of Wing Aspect Ratio and Shape, *51st AIAA Aerospace Sciences Meeting including the New Horizons Forum and Aerospace Exposition*, 2013. Grapevine, Texas.

[10] Phillips, N., Knowles, K. & Lawson, N., Effect of wing planform shape on the flow structures of an insect-like flapping wing in Hover, *27th International Congress of the Aeronautical Sciences. ICAS*, 2010. Nice, France.

[11] Shahzad, A., Tian, F., Young, J. & Lai, J., Reynolds Number Effects on the Aerodynamic Performance of Wing Planform Shapes in Hover, *19th AFMC*, 2014. RMIT University, Melbourne, Australia.

[12] Tian, F.-B., Dai, H., Luo, H., Doyle, J.F. & Rousseau, B., Fluid–structure interaction involving large deformations: 3D simulations and applications to biological systems, *Journal of Computational Physics*, **258**, 2014, 451-469.

[13] Wilkins, P.C., *Some unsteady aerodynamics relevant to insect-inspired flapping-wing micro air vehicles*, Cranfield University, UK, 2008.